7th ECCOMAS Thematic Conference on Smart Structures and Materials
SMART 2015
A.L. Araújo, C.A. Mota Soares, et al. (Editors)

NUMERICAL SIMULATION OF BEHAVIOUR AND EXPERIMENTAL VERIFICATION OF PNEUMATIC AND SMA ACTUATORS IN HYPER-MOBILE PNESTIFMATIC JOINT

E. Prada[*], M. Valášek[*], G. Granosik[†]

[*] Czech Technical University in Prague
Faculty of Mechanical Engineering,
Vehicle Center of Sustainable Mobility
VTP Roztoky, Přílepská 1920, 252 63 Roztoky u Prahy, Czech Republic
erik.prada@yahoo.com, michael.valasek@fs.cvut.cz

[†]Technical University of Lodz
Faculty of Electrical, Electronic, Computer and Control Engineering
Institute of Automatic Control
B. Stefanowskiego 18/22, 90 924 Lodz, Poland
granosik@p.lodz.pl

Key words: Hyper-mobile joint, Redundant mechanism, Pneumatic bellows, SMA actuators.

Summary: *Hyper-mobile joints have application in various mechanisms in which it is required to have a considerable ability of manipulability with the greatest degree of freedom possible. In our case, the PNESTIFMATIC hyper mobile joint is used as a main component of a hyper redundant robotic manipulator. The original joint mechanism is based on a US6870343 B2 patent draft, which was subsequently extended by a platform for more precise positioning and correction of the overall stiffness. Correction mechanical members and actuators consisting of SMA springs were added into the mechanism. Main content of the article is dedicated to numerical modeling, pneumatic bellows and experimental verification of SMA hyper mobile joint actuators. Numerical modeling consisted of FEM analysis of a pneumatic bellow in SolidWorks programme, in which non-linear dynamic task was solved. Hyper elastic Money Rivlin model was considered within the process of solving of this task. Definition of Rayleigh damping coefficients according to the work of Chowdhury and Dasgupta was also considered. Shift, velocity and acceleration values of expansion of pneumatic bellows were drawn from post processing. In the section dedicated to experimental verification of SMA actuators, verification of various SMA springs with different stiffness coefficients was carried out. It helped us to obtain dependencies of shift on the supply current and values of the induced forces.*

1 INTRODUCTION

Mechanism, from which the high level of maneuverability is expected, is classified as hyper - redundant. The concept of redundancy can be seen in the dissertation thesis of Gregory S. Chirikjian with the title "Theory and application of hyper-redundant robotic manipulators", in which he discusses kinematic analysis, simulations and designs of hyper-

redundant manipulators [1]. This mechanism can have a form of the certain type of joint, which enables excessive maneuverability of mechanism, thanks to its mobility. Researchers have begun to examine redundancy in the sixties of the 20th century. They mostly focused on the category of robotic manipulators. Pioneers of this field were Victor C. Anderson and Ronald C. Horn [2] with their manipulative device called Tensor-Arm, which was subsequently patented. Principle of this device lied in contraction of synthetic ropes and tilting of individual segments with usage of transmission mechanisms to the specified side. Later, combined methods of generation of the action force, for example by usage of the pneumatic actuators, have begun to be used. Most of these mechanisms were based on serial connection of individual structural parts. Only in the beginning of the nineties, parallel design has begun to be used. Difference between parallel and serial arrangement of the main structural frame lied in the possibility of the application of actuators in "side by side" segment. This contributed to greater precision of manipulation and higher reliability of the whole system.

Similar hyper-mobile mechanical system was built and patented by Johann Borenstein and Gregorz Granosik [3]. Their joint was practically used in the construction of the hyper mobile snake-like robot called OmniTread at University of Michigan. OmniTread consisted of the same segments and hyper mobile pneumatic joints, while for its crawling movement, it used special action device mounted on the sides of the segments. On the basis of the mutual cooperation, we have therefore decided to improve this joint, which led to designing of the PNESTIFMATIC joint.

2 GENERAL SPECIFICATIONS OF PNESTIFMATIC JOINT

The basic PNSTIFMATIC joint is constructed of three chambers separated by support baffles. Each of the chambers has its functional justification that is based not only on the physical principle, but also on the different material construction. Although the resulting functionality of every part is highly specific, in the final analysis it is assumed that all structural parts will be symbiotic. Structural parts of the joint can be therefore divided into support-linking elements, control, regulatory, sensor and other electronic components with actuators.

2.1 Support-linking structural elements

The task of support-linking elements is primarily to create the supporting framework of the joint. These elements are formed by:

- The universal joint - the main function of which is to connect the main baffles and achieve the carriage of rotary action in two planes.
- three separating baffles- each of them has different shape, while the most important are the internal baffles separating pneumatic bellows from other chambers. Baffles serve as the support element for attachment of the pneumatic bellows, joints, actuators, stick of distance, correction clamps and coils. These baffles are also structural parts, which are intended to be produced from aluminium material.
- connecting shaft- which serves to connect the universal joint with the baffle and axial support joint. This structural part is intended to be produced from a suitable structural steel.
- Supportive axial joints - their main role is the ability to perform a tilting movement together with the baffle. Supportive axial joint creates a function of the main supportive element between the connecting shaft and the last baffle that can be tilted

in the desired direction. The function of the axial joints that are connected by clutch with the shaft of each electromagnetic actuator is to correct the tilt of the last baffle and transportation of the action power of electromagnetic element.

- Stick of distance -which form a supportive function between the baffles.
- Correction clamps - the purpose of which is to attach the electromagnetic actuators to the separating baffle, while production of tailor-designed parts is also considered.

2.2 PNESTIFMATIC joint actuators

The main task of the structure actuators is to create the required action force:

- Pneumatic bellows - their function is to produce the power effect in the direction of the bellow´s expansion. In effective combination and with the appropriate treatment with restraint rings and nylon anti-wear skin, they can perform cyclic power effect without significant wear. Pneumatic bellows therefore perform the opposite action as in pneumatic muscles, in which contraction is performed. Pneumatic bellows are created of a specific type of rubber, which guarantees the hyper-elastic properties needed. What is also important is their geometrical shape, length, thickness and diameter. PNESTIFMATIC joint contains four symmetrically arranged bellows, which have parallel planes of symmetry to the planes of universal joint rotation. Border areas of the both ends of the bellows are attached to the intermediate baffles, while there is an opening for connection of the outputs of pneumatic regulators on each of the sides of the bellow.
- Electromagnetic actuators - their task is to generate the pushing or pulling force needed to transfer through supportive axial joint and they act at the final baffle, which results in its tilt into desired angle. Electromagnetic actuator can be additionally equipped with the position of the rod sensor. That is why we can use such actuator not only to accurate positioning but also for counterforce action.

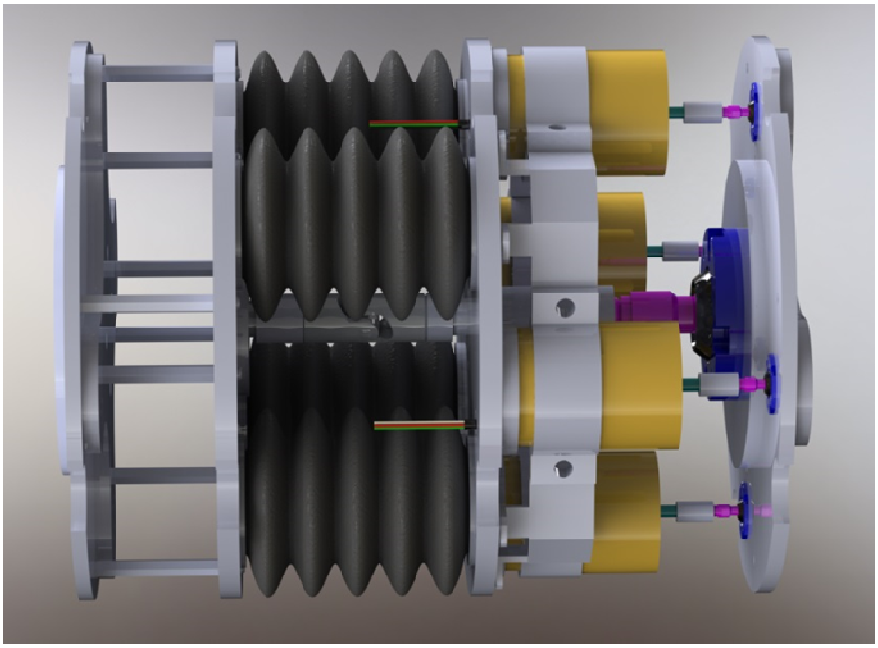

Figure 1: 3D view of design PNESTIFMATIC joint in SolidWorks 2014.

2.3 Control, regulatory and sensor components

The last important category of the PNESTIFMATIC joint consists of control, regulatory, sensor and other electronic components. These consist of:

- Pneumatic regulators - they provide the regulation of pressure on desired level for each of the pneumatic bellows.
- pressure sensors- their task is to sense the pressure in each of the bellows, therefore they are important part of the feedback regulation.
- Printed circuit boards with microcomputer - microcomputer is used to generate the control signals for pneumatic and electromechanical actuators. Moreover, printed circuit board includes other components needed, such as operational amplifiers, power transistors in Darlington connection, voltage regulators, power connectors, sockets and others.

3 The basic description of the PNESTIFMATIC joint mechanics

PNESTIFMATIC joint has been designed in such a way to be able to perform the movement in the 3D environment. Functionally, the most important part is the chamber, in which pneumatic bellows are situated. These bellows can act with the biggest strength to other segments within the whole redundant system. Torque effect is created by the combination of adjustable positioning of universal joint which allows rotation in two planes and applied force of the expansion pair of bellows. It is possible to determine the size of this effect using the following equation [4]:

$$M_p = \frac{D}{\sqrt{2}} A\left(p_{Acel} - p_{Bcel}\right) \tag{1}$$

where D is the distance from the central axis of the segment to the central axis of the given pneumatic bellow, A is the capacity of the cross section of the bellow, $p_{Acel} - p_{Bcel}$ is the difference of pressures of the opposing bellow pairs. Area with pneumatic bellows and universal joint has two degrees of freedom of movement. Steering angle of the pneumatic part of the joint depends on several factors. One of them is the total expansion and compression length of the bellows possible, material from which the bellows are made (whether corrective supplements such as restraint rings or central handles were used), which possibilities of rotation the universal joint allows and also the expansion pressure in the bellows. On the basis of the experimental verification, we can most plausibly determine the maximum and minimum space that will be created when approximating or distancing of separating baffles. The process of obtaining the specific rotation of the pneumatic part lies in the suitable control of the pneumatic actuators. Physically it is about the control of the expansion pressure in bellows (when bellows are pressed to a certain value of pressure, we can obtain the expansion shift needed). Mechanically, such shift to the entire joint is expressed by torque effect M_p, however we cannot forget about when describing the overall mechanics of the joint [5]:

- moment of inertia I of the parts rotating around the centre of the universal joint
- angle of semi-rotation of a pneumatic part $\ddot{q}$
- torque M_s around the centre of the rotation of a universal joint caused by the elastic properties of the inflated bellows
- torque M_m, which is a result of the effect of weight of the angles raised above the ground.

3.1 Determination of the dynamic equation of PNESTIFMATIC

Now, that we know all the acting force effects, we can define the dynamic equation that can be later used for the management:

$$I\ddot{q} = M_p - M_s - M_m \tag{2}$$

The basis lies in the management of the appropriate pressure for the pair of opposing bellows. Toughness greatly affects this device, because it can be influenced by the change of the pressure difference. The greater precision we want, the tougher the system must be and vice versa - if there is a certain flexibility of the system required, it is convenient to limit it. Management of the pressure regulators can be done with the help of pulse width modulation that can achieve the desired pressure. From the experimental results of Granosik and Bornstein we know that with a decreasing toughness of the system, this phenomenon negatively affects the positioning [5].

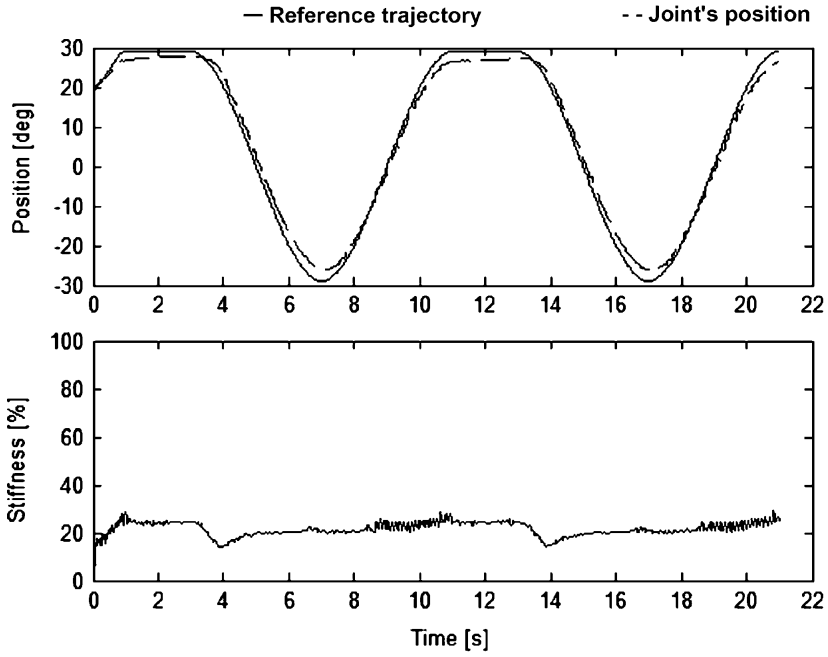

Figure 2: Experimental results in positioning proces and stiffness when applying the algorithm PPS (Granosik and Borenstein 2005) [5].

In order to increase the positioning accuracy and reduce the impact of toughness in moments where excessive flexibility is undesirable, we have extended the original patent on the platform with electromagnetic actuators. This usage in the design also ensured the higher level of maneuverability due to the use of the handle in form of the axial joint. Restriction of the baffle´s movement in spherical coordinates was secured by foursome of the links of rods of the electromagnetic actuators and additional axial joints. Tilting movement is therefore created by the activity of rods of the electromagnetic actuators. Maximum angle of titling therefore depends on the relative length of the last two baffles of a joint as well as on the length of the affecting rod. PNESTIFMATIC joint has a total of six degrees of freedom of movement and there is a large number of positions that may be acquired in space. In the following Figure 3, Figure 4 and Figure 5, we will present the extreme positions that can be achieved for various configurations.

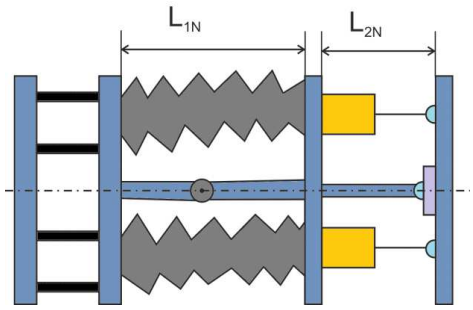

Figure 3: Schematic representation of the position of joint PNESTIFMATC in the initial state.

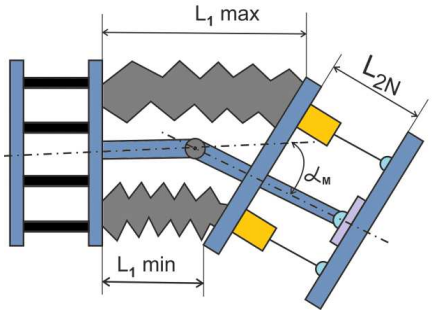

Figure 4: Schematic representation of the extreme position of joint PNESTIFMATC after time when bellows worked.

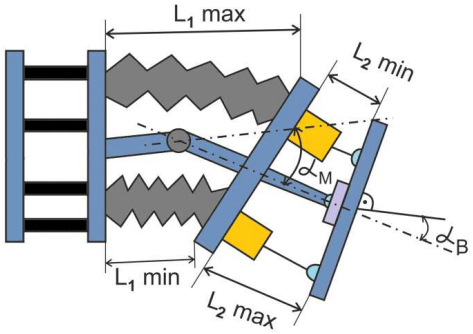

Figure 5: Schematic representation of the extreme position of joint PNESTIFMATC after time when bellows and electromagnetic actuator (or SMA actuator) worked.

Overall positioning of the redundant mechanism therefore depends on the position of each of PNESTIFMATIC joints in the mechanical chain. By combining of these movements with the appropriate management, we can achieve the movement with a considerable degree of maneuverability. In Figure 6, we can see the 3D model of redundant mechanism with 30 degrees of freedom (DOF). In terms of management, this system is a overactuated mechanical system. Real model must also include additional components such as pneumatic tubes for the airflow, regulators and electronic components for connection of the electromagnetic actuators.

Ultimately, we consider creating a mechanic system that would basically link the advantages of fixed as well as mobile redundant systems in the future. Such systems could be named the Universal redundant mechanical systems (Uni-redundant mechanical systems).

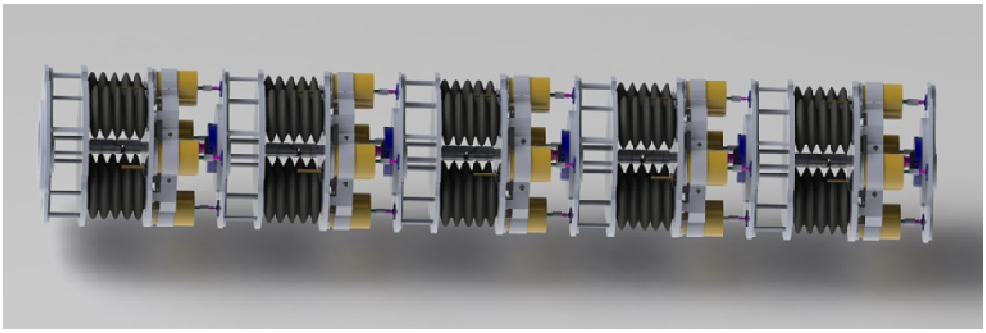

Figure 6: 3D model of redundant mechanical system.

4 NUMERICAL SIMULATION OF THE BEHAVIOUR OF PNEUMATIC RUBBER BELLOWS

Before the simulation itself could have been performed, we proceeded to create a virtual model in SolidWorks 2013. More specifically, it was a pneumatic bellow McKibben, the same as the one used in the case of US 6,870,343 B2 patent. The design parameters of a virtual model were consistent with a realistic model which allowed us to approximate to the truest conditions within simulation. The actual simulation consisted of verifying the behaviour of a pneumatic bellow under certain pressure. It means the change of affection of individual tenseness in mechanism, the change of the size and speed. Because of this, the problem of nonlinear dynamic load was solved within simulation. In order for us to be able to simulate the possible impact of the bonds, we have defined the limits consisting of contacts on the both ends of the pneumatic mechanism. During the attempt to implement restrain rings to a simulation model, the frequent fall of the computational core occurred. We suppose that the reason for these falls was the considerable complexity of calculation during the contact of the surfaces.

The great disadvantage of the simulation of this type is a relatively time-consuming severity of the calculation itself. The increase of the required time is manifested mostly in components with intricate geometric shapes. In our case, the geometric complexity itself necessitated a minimum density of mesh required from the generator. The calculation of each simulation was conducted on a special calculating virtual machine with four shared cores (Intel Core I7) of processors with active hyperthreading. For the needs to store the operational data, the virtual computer was equipped by 8 GB of memory. Important parameter for the successful implementation of the calculation in terms of the resources provided was the size of the virtual disk's capacity available. Mostly in the cases in which the calculation with a defined adaptive action of individual iterations was performed, there was a great demand for storage space. The time period of calculation of these adaptive steps have increased mostly in the cases where the possibilities of usage of hyper-elastic material properties were verified. All changes of settings and procedures relating to individual phases of simulation will therefore be introduced in separate subchapters.

In addition to the standard model of the pneumatic bellow, we tried to verify the extended model in our simulation as well. This model also included the restraint rings anchored in the individual waves of the mechanism. The function of these rings was guide the expansion pneumatic bellow. From the course of the simulations we have discovered that the usage of

other structural elements within one simulation is extremely demanding for computing power as well as for the overall time that equals to tens of hours. For this reason, we carried out the simulations of the design elements separately in the final stage.

4.1 Order of steps in the phase of pre-processing and the adjustment parameters

This simulation part is very important in terms of the correct entry of the input calculation parameters. Otherwise, the bad interpretation of incorrect results could occur as the result of wrong input parameters. In the worse case, the computational core could fall. As mentioned in the previous chapter, in our case we will observe the change of behaviour of the pneumatic bellow under the influence of the input pressure. Total number of pressures, which will be observed, corresponds to the number of pressure changes at experimental part of verification, see Table 1.

Number of simulation	1.	2.	3.	4.	5.	6.	7.
Max bellow pressure (MPa)	0,006	0,042	0,065	0,113	0,142	0,192	0,238
Number of simulation	8.	9.	10.	11.	12.	13.	14.
Max bellow pressure (MPa)	0,284	0,332	0,380	0,424	0,470	0,516	0,602

Table 1: Values of pressure for simulation process

At first, we have chosen a nonlinear dynamics problem to be solved and from the individual parts of simulation model, we have chosen pneumatic bellow to create a shell element. It is the solution of shell element what guarantees us more simple numerical calculation. Some reports however indicate that when dealing with pneumatic mechanisms, the non-shell element should be used, because the thickness of a shell is the same in the whole object, while non-shell element can reflect realistically the actual change of the thickness in the places of bending, see Figure 7 [6].

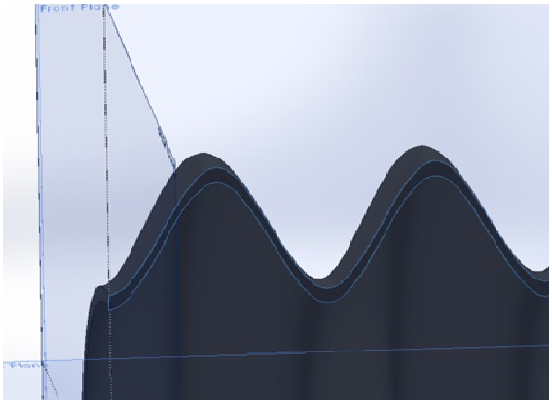

Figure 7: Illustration of the varying thickness of individual waves of the pneumatic bellow

In the second step, we have defined the material properties of simulation model. Since the simulation model consists of two different geometrical and material elements we have defined the material for every structural element separately. This definition consisted in selecting the material generated by us. More specifically, it was a type of hyper-elastic material Mooney-Rivlin, which was applied to the shell element of pneumatic mechanism. Following applies for the strain energy and the density of this type of material:

$$W = C_1\left(\overline{I}_1 - 3\right) + C_2\left(\overline{I}_2 - 3\right) \tag{3}$$

where C_1 and C_2 are empirical suitably chosen material constants, and $\overline{I}_1$, $\overline{I}_2$ are the first and the second invariant of unimodular Cauchy-Green components of the deformation tensor.

$$\overline{I}_1 = J^{-2/3} I_1,\ \overline{I}_2 = J^{-4/3} I_2 \tag{4}$$

$$I_1 = \lambda_1^2 + \lambda_2^2 + \lambda_3^2 \tag{5}$$

$$I_2 = \lambda_1^2\lambda_2^2 + \lambda_2^2\lambda_3^2 + \lambda_3^2\lambda_1^2 \tag{6}$$

$$J = det\left(\boldsymbol{F}\right) \tag{7}$$

F equals to deformation gradient. Due to the fact that the characteristic attribute of our material is its incompressibility, $\mathrm{J} = 1$. Based on the works [7] the appropriate material constants were chosen: $\mathrm{C}_1 = 1\,(\mathrm{MPa})$ a $\mathrm{C}_2 = 0{,}9\ (\mathrm{MPa})$, while the condition $\mathrm{C}_1 + \mathrm{C}_2 > 0$ had to be fulfilled. In XY plane, the specific value 0,4999 have been chosen as Poisson's ratio, because of its compatibility with the settings of the computational core (for the cases of shell elements with great displacements). We have chosen the standard aluminium material as our second structural element in a simulation model.

In the next step, we have defined the conditions of the anchoring of shell element of a bellow in such a way, that it will comply with the real attachment in the structural model. Since we focused on the simulation of the pneumatic bellow itself, the anchoring was carried out at the edge of a shell element in the same way as if it was physically glued to the clip anchor. From the opposite side of the mechanism, the bond between the clip anchor and pneumatic bellow was defined. The reason for using a clip anchor in simulation was to achieve the limitation of expansion caused by the influence of pressure in the places of gluing, as well as the simulation of the certain mass, although only a symbolic one.

In this fourth step, the input values of expansion pressures have been sequentially defined. They have been changing in accordance with the values in the subsequent real experiment. Simulation behaviour was examined sequentially for each initial pressure change. Since we know that a certain pressure in pneumatic bellow is achieved in nonlinear converge, for each case of pressure custom accrual curves have been defined. These have been used in setting of the pressure parameters Table 1.

The fifth step is to define Rayleigh damping coefficients. The reason why we consider this influencing factor is that we assume some damping properties of a rubber pneumatic mechanism. Since the simulation model consists of two components with different material composition and geometrical shapes, there is an assumption of mutual influence of the masses during the expansion of a mechanism. Rayleigh´s damping is defined by the following matrix entry:

$$\boldsymbol{C} = \alpha \boldsymbol{M} + \beta \boldsymbol{K} \tag{8}$$

Where **C** is the damping matrix of physical, **K** is the stiffness matrix, and **M** is the mass matrix. In many cases of calculations, it is advised to neglect the coefficients α, which together with the stiffness matrix have influence in form of the friction effect of a mass. The algorithm from the work of Chowdhury and Dasgupta [8] allows us to express both α and β coefficients, whose application is important especially in cases with a high degree of vacancy of a mechanical system. The following applies for the coefficient β:

$$\beta = \frac{2\zeta_n \omega_n - 2\zeta_1 \omega_1}{\omega_n^2 - \omega_1^2} \tag{9}$$

where ω_n is the n-th natural frequency or the harmonic frequency, ω_1 is the smallest natural frequency of the structural part, ζ_n is the damping factor for the n-th natural frequency and ζ_1 is the damping factor for the lowest natural frequency. By subsequent substitution of β parameter into Equation 10 derived from Equation 8, we can express the coefficient α.

$$2\zeta_n \omega_n = \alpha + \beta \omega_n^2 \tag{10}$$

Thus obtained coefficients α and β may be installed into the program in appropriate setting. In our case, we needed to at first determine the natural frequencies of the pneumatic mechanism in order to determine these coefficients. Because of this reason, before the simulation of the dynamic behaviour of a pneumatic mechanism, we needed to perform frequency analysis of the pneumatic mechanism. From the results of this analysis, we obtained natural frequencies and corresponding custom shapes. The values of the damping factors were used according to the works [9].

We have defined the damping factor $\zeta_n = 0,05$ for the frequency $\omega_n = 21,602\left(rad.s^{-1}\right)$ as the largest frequency of the frequency analysis. The damping factor $\zeta_n = 0,01$ was defined for the lowest frequency $\omega_1 = 3,4703\left(rad.s^{-1}\right)$. After the substitution into the equations, the calculation of the coefficients was as follows:

$$\beta = \frac{2 \times 0,05 \times 21,602 - 2 \times 0,01 \times 3,4703}{21,602^2 - 3,4703^2} = 0,00460 \tag{11}$$

$$\begin{gathered} 2 \times 0,05 \times 21,602 = \alpha + 0,00460 \times 21,602^2 \\ \alpha = 0,01365 \end{gathered} \tag{12}$$

We were able to substitute the resulting values of coefficients α and β into the formulas in SolidWorks environment.

In the last point of the pre-processing part, we proceeded to set the parameters of finite elements mesh. In examining the characteristics of the geometry of the pneumatic bellow we concluded that the best option is to choose the possibility of the mesh construction based on the curvilinear approach. It means that the resulting of finite elements mesh will automatically compress in places where there is a curvature of the given object. In our case it causes that generator of the mesh created a denser mesh in the areas of the mechanical waves. More specifically, the dimension of approximately MAX 3,505 (mm) was defined for the maximum size of the element. For the minimum size, the dimension of approximately MIN

1,168 (mm) was defined. Enhancement factor of individual elements was set to a value of 1,5 and the minimum number of elements in the circle was set to 8. We selected the number of integration points to 16 in the extended parameter settings of the mesh generator. These points are used to control the level of distortion of tetra hydric elements. The final shape of the model with a finite elements mesh is shown in Figure 8.

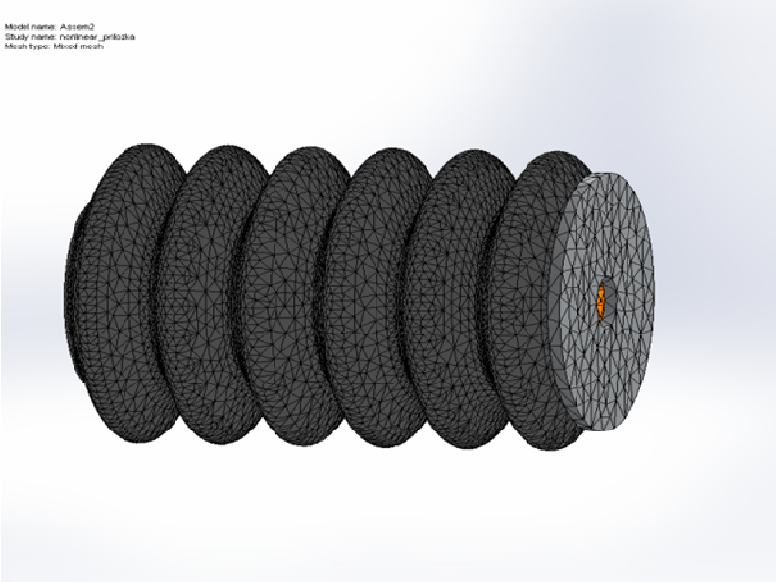

Figure 8: Correct finite element mesh on the pneumatic bellow

4.2 Processing phase

After careful setting of all necessary parameters of pre-processing phase, we proceeded to the actual solving of the problem of non-linear dynamics of pneumatic mechanism. Before starting the SolidWorks program solver itself, we set the parameters of this solver. In Figure 9 the possible settings of the computational core are depicted.

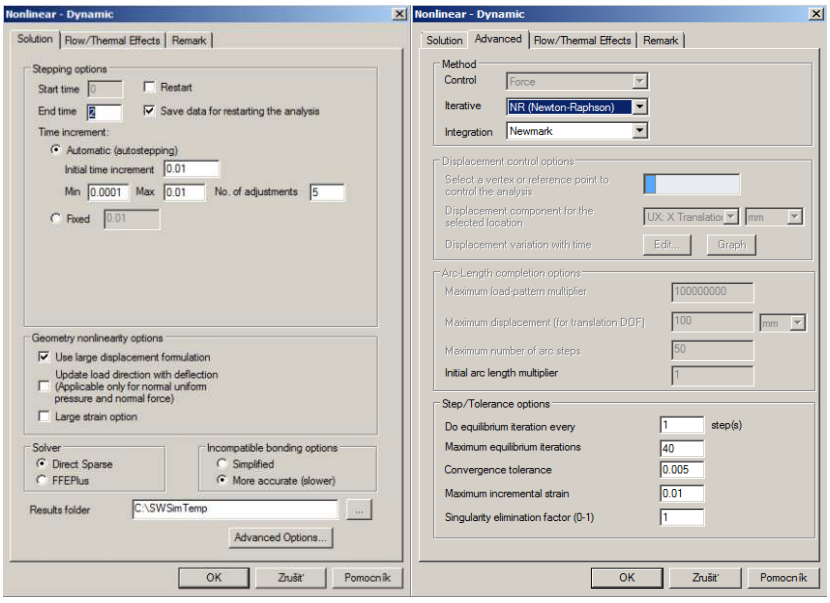

Figure 9: Setup windows of the solver part in the SolidWorks

In "*Stepping options*" part, we set the finish time of the calculation to 2 seconds, which roughly corresponds to the time of experimental verification. At that time, the settling of expansion of the mechanism at a given pressure occurs. In the subsection "*time increment*" we have chosen the "*auto stepping*" of individual frames due to non-linear change of the mechanism's shape. In the following section "*Geometry nonlinearity options*" we have chosen the option of large displacements, while hyper-elastic material is supposed to experience major changes of shape. It was also because of this reason, that we have chosen Direct Sparse in the section for selection of computational core "*Solver*". "*Direct Sparse"* was chosen for the direct solution of sparse matrices, which is suitable for the solution of problems with a high degree of shifts. Algorithms for the solution of sparse matrices are much more time-consuming than in the case of dense matrices, which results in the overall time complexity of this problem's calculation. Due to the existence of contact of two structural elements of the whole simulation model, in "*Incompatibile bonding options*" we have chosen the option of more accurate (slower) calculation process for the case of touching areas. In the advanced settings of computation core, the Newton-Raphson method with Newmark integration has been chosen. Since in previous experiments of this calculation, the fall of computational core occurred mostly at the end of the calculation, we modified the value of maximum equilibrium iterations to 40 and reduced the value of tolerance to 0,005. After all these settings, we decided to run the calculation for each pressure change according to Table 1.

4.3 Results of the simulations of the post-processing phase

After performing the simulations, we have created graphical outputs of displacement, tenseness, deformation, velocity and acceleration according to the pressure changes listed in the chart. To illustrate the following outputs of simulations we have chosen one threshold value of pressure.

In Figure 10, the displacement of pneumatic bellow at 2 seconds since the beginning of the expansion is depicted. More specifically, we can see the maximum expansion and at the same time its displacement at the place with splice plate. Chromatic shift corresponds to the assumption that the pneumatic bellow will primarily expand in the x axis direction. The area with the lowest shift is very close to the area of anchorage of shell element. It can be concluded from the characteristic shape after the expansion that if the restraint rings were present in the calculation, the maximum length of the expansion would probably be even few millimeters greater.

Figure 11 shows the distribution of the reduced stress according to Von Mises-Hencky stress theory. The most significant effect of stress occurs in the areas of bending of the individual waves of pneumatic bellow. This means that during the expansions of the bellow, the waves expand in the direction of the x axis and at the same time, the diameter of the bellow increases. The result is the expansion of the bellow in all directions within the possibilities of the material. The depicted tenseness is the consequence of the impact of the planar tenseness in the shell. Another important information that we have obtained from the simulation is a representation of the pneumatic bellow´s deformations in Figure 12. The greatest deformations occur in the waves that are closer to the central axis of the bellow. The reason for this is that during expansion of the bellow, the individual fibers of the material stretch along the shell element which manifests in the increase of the area. Subsequently, this area adapts to the affecting pressure in the given areas, provided that no limiting element works against the expansion.

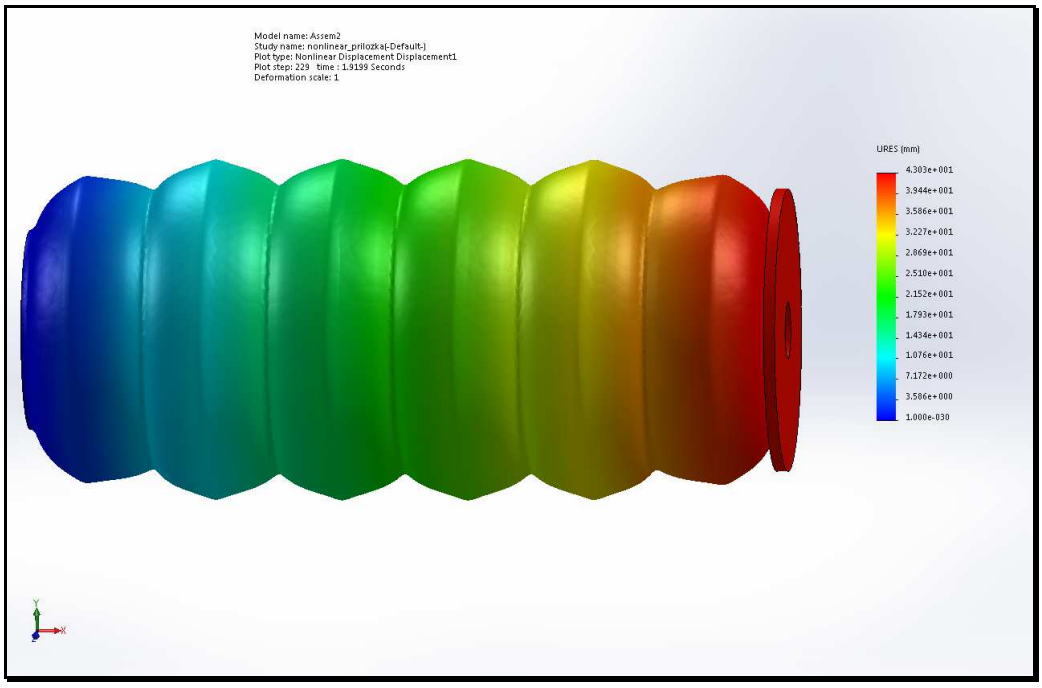

Figure 10: Graphical representations of pneumatic bellow displacement with 0,6 (MPa) bellow pressure

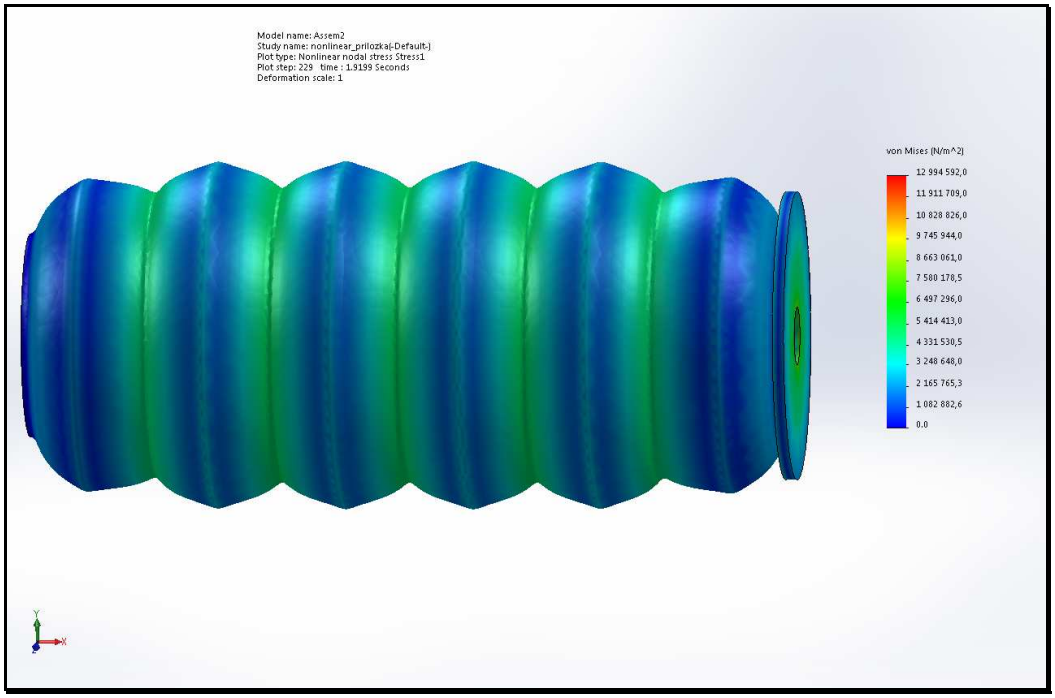

Figure 11: Graphical representations of pneumatic bellow stress effect with 0,6 (MPa) bellow pressure

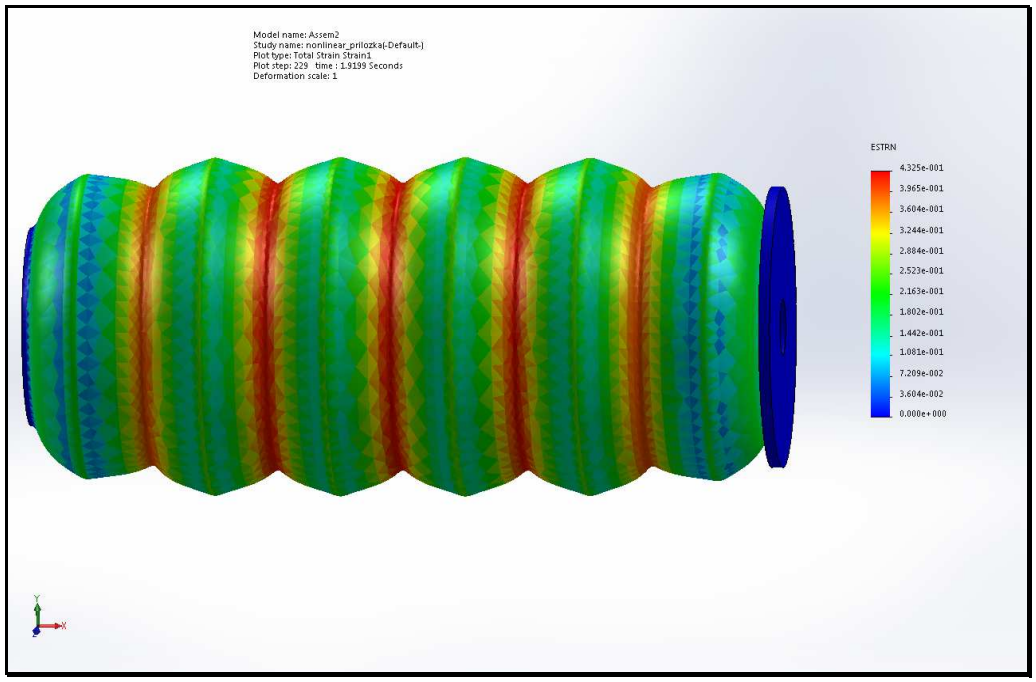

Figure 12: Graphical representations of pneumatic bellow strain deformation with 0,6 (MPa) bellow pressure

Thus, for example the deformation close to the areas of constraint and contact with the plate is smaller, since the material is trying to preserve the original geometric shape in the near surroundings. We can achieve the lowering of deformation in the areas of lower folds thanks to the restraint rings added to the structural design of restricted expansion of pneumatic bellow.

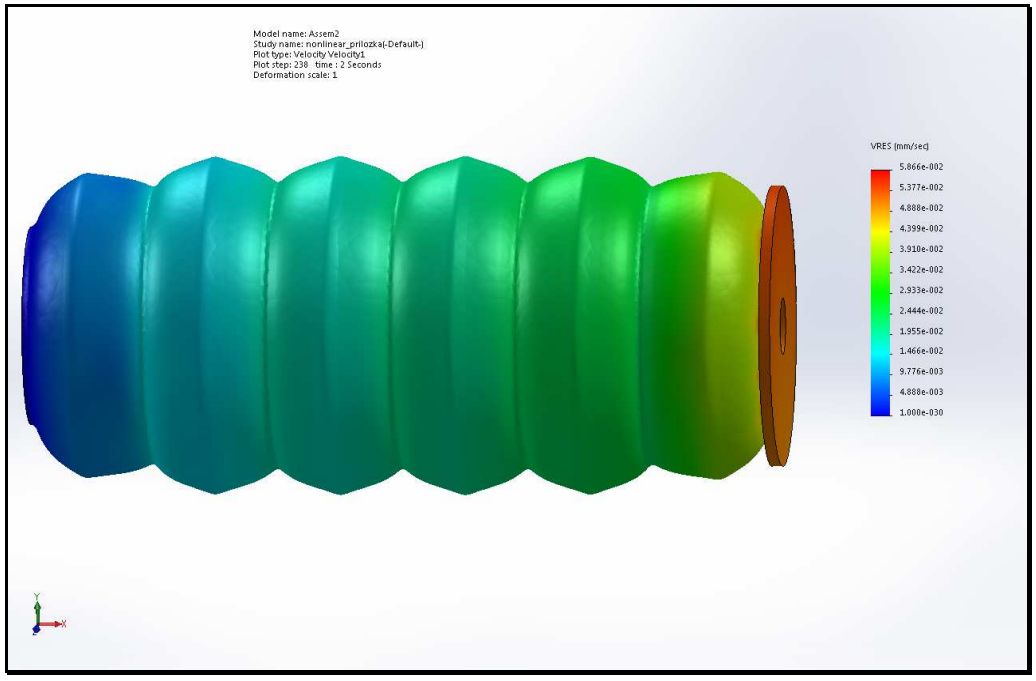

Figure 13: Graphical representations of pneumatic bellow velocity of expansion with 0,6 (MPa) bellow pressure

In another Figure 13 we can see the progress of velocity of individual parts of the bellow. Since the figure represents the final moment of simulation (final time interval) it is understandable that the velocities expressed are smaller compared to the velocities in the earlier time intervals. However, the character of the change of velocity along the bellow is maintained. It can be clearly seen there, that more distant parts with the splice plate have higher velocity than those which are closer to constraint.

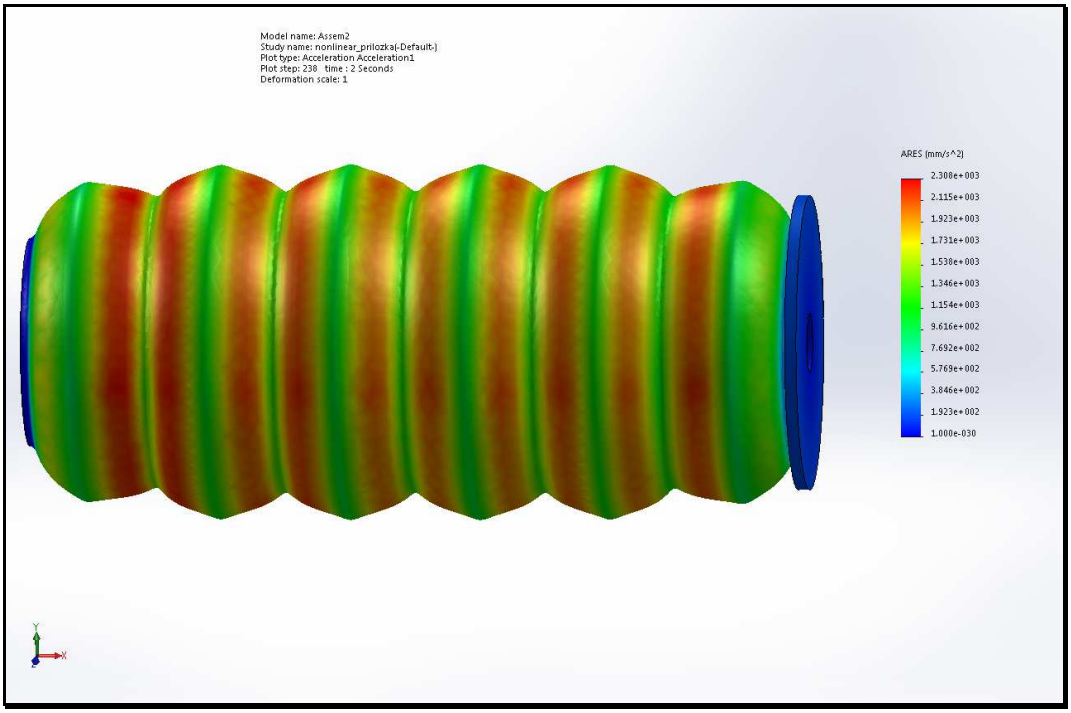

Figure 14: Graphical representations of pneumatic bellow acceleration of expansion with 0,6 (MPa) bellow pressure

The last variable that we were interested in during the post-processing of the simulation and its final time interval was acceleration. From Figure 14 we can conclude that the areas with the greatest acceleration are on flat surfaces which join the individual waves of the pneumatic bellow. Those areas have the greatest tenseness.

4.4 Summary

In conclusion, we will summarize the results of simulations at different expansion pressures and in different time intervals. In Figure 15, we can see the overall dependence of the change in increase of the shifts for individual expansion pressures of pneumatic bellow at time interval corresponding to the total simulation time. From the shape of the graph it can be seen that with the increase of pressure, the final displacement of the pneumatic bellow also increases. Only at higher temperatures, the bellow begins to expand considerably. At the highest pressure values, the expansion increases, but again, sporadically.

In Figure 16, the dependence of the speed of expansion of the bellow on the pressure and time of the simulation is depicted. Noticeable increases of speed are present in initial and medium simulation times, when the settling of the pressure in the bellow is expected.

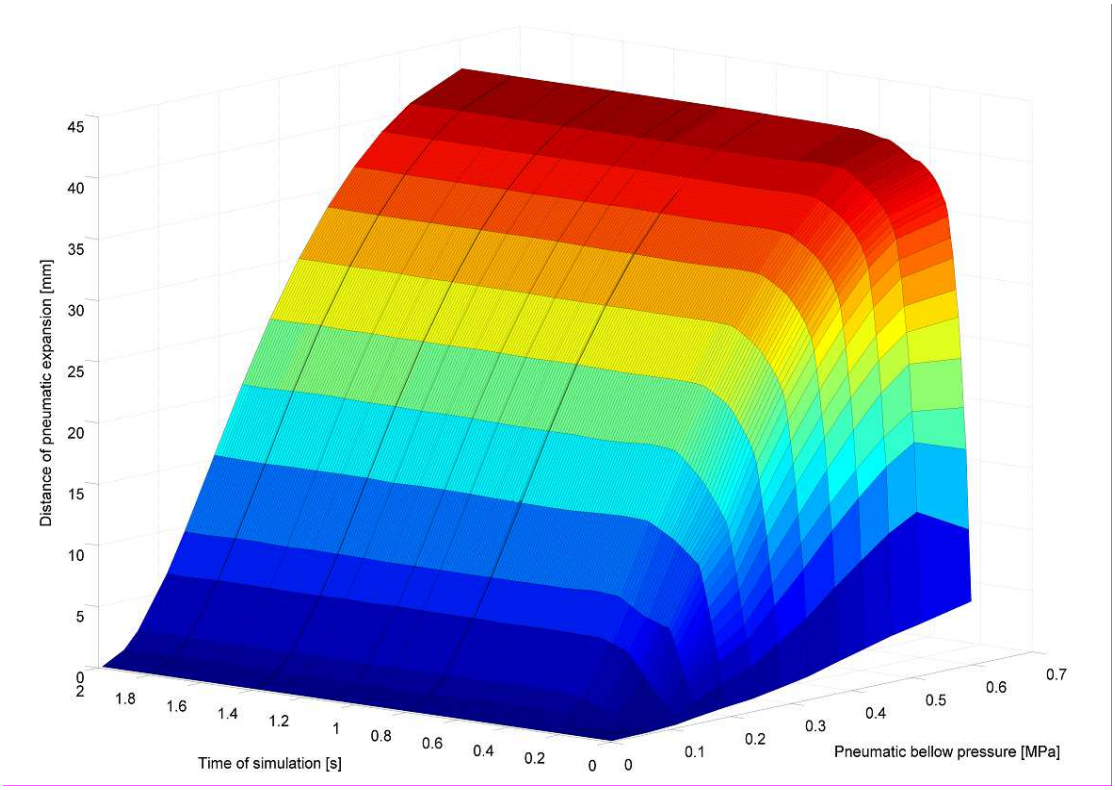

Figure 15: The variation of displacement in the pressure change during the simulation period

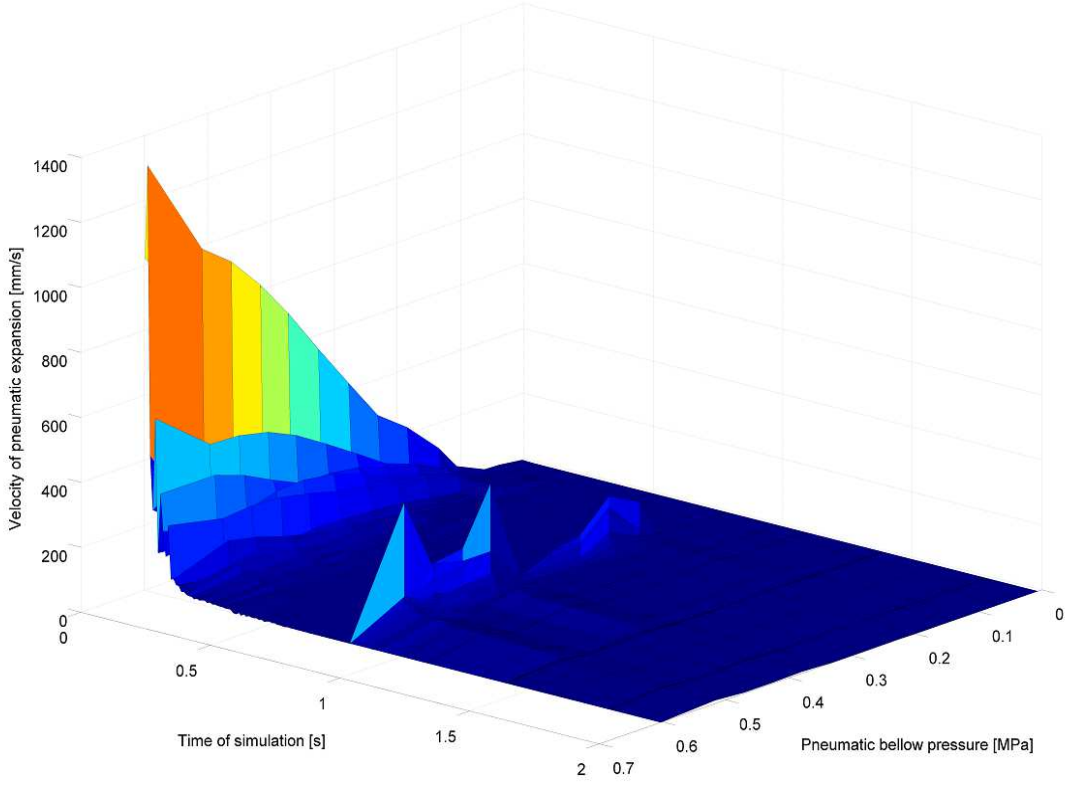

Figure 16: The variation of velocity in the pressure change during the simulation period

5 EXPERIMENTAL VERIFICATION OF SHAPE MEMORY ALLOY SPRINGS FOR PNESTIFMATIC JOINT APPLICATION

In the previous chapter, we presented a numerical simulation of the most important part of the action component of the PNESTIFMATIC joint. In case of the application of PNESTIFMATIC joint positioning, we can use two variants of springs - contractive and expandable for more accurate positioning of the SMA spring. The role of the SMA actuator is to build the Force . We have therefore experimentally verified both variants of SMA springs. We have connected the contractive spring from

Nitinol to the power supply. Contraction of the spring has been verified at various loads which impact on the spring in form of various weights. After connecting of individual weights from 50 to 500 grams, with 50 grams increase, we have changed the voltage up one volt until we were able to monitor the contraction of the spring. At the same time, we have recorded the values of currents that went through the spring. Results were expressed graphically in the following dependencies of the contraction shift on the change of currents for one specific force action, see Figure 17.

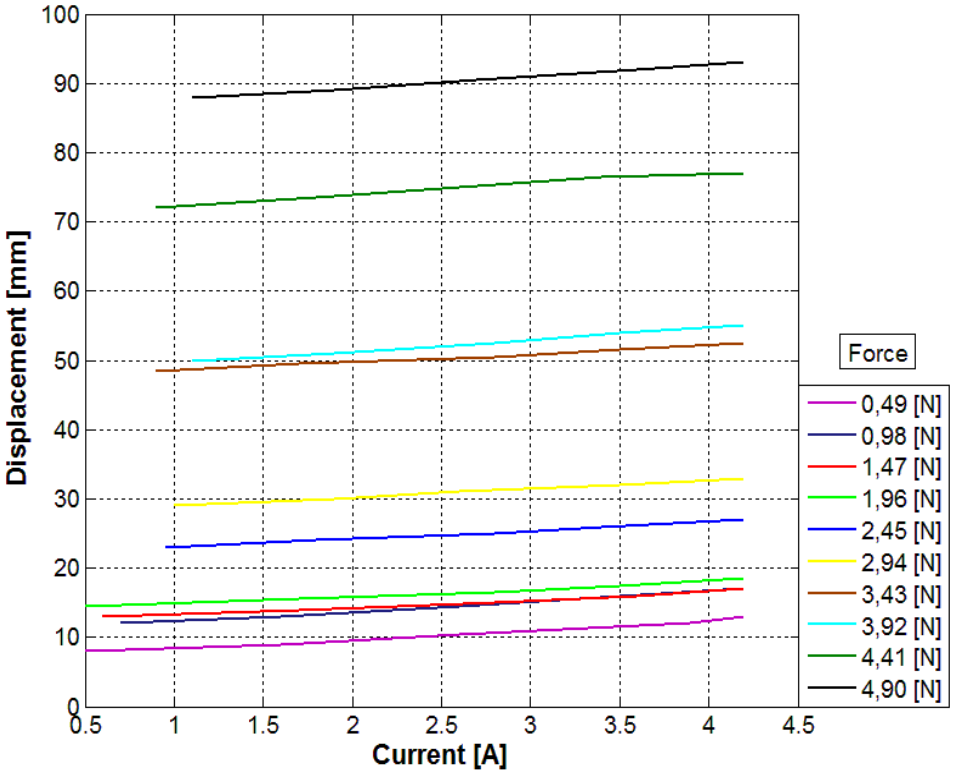

Figure 17: One-way memory effect and two-way memory effect

From these results, we can conclude that the characteristics have a linear character. It means that by using of regression of the values obtained, we can gain a relationship from which we can determine the current of the power supply for the specific shift.

In the second measurement, we have investigated the expansive spring from Nitinol, initial length of which was 26 (mm). Unlike the first case, the measurement was realized in such a way, that we inserted classic steel springs with the following stiffness coefficients: k_1= 309,13; k_2=177,34; k_3=351,67; k_4=343,21 a k_5=308,82 into the spring from Nitinol.

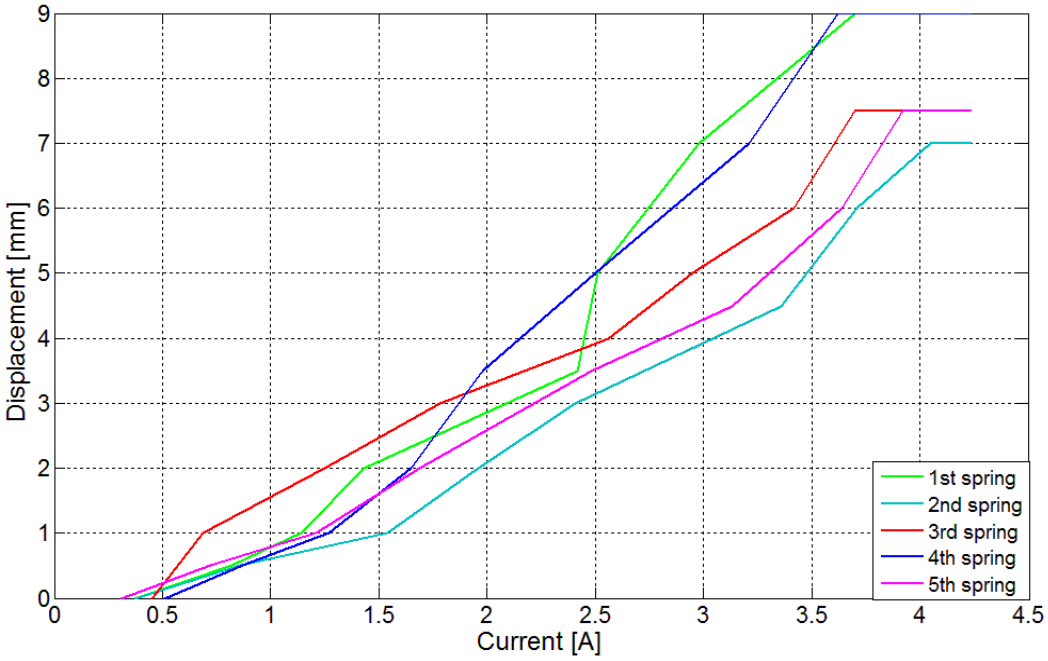

Figure 18: One-way memory effect and two-way memory effect

We have therefore achieved the reverse counteraction towards the spring from Nitinol, when the current was passing through it. As in the previous case, we have also changed the voltage, in the interval from 0 to 2 (V). However, with a range of step of 0,2 (V). Together with the change of the voltage, we have measured the current passing through the spring as well as the size of deflection of the spring. The results of the measurements are depicted in Figure 18.

Graphs of dependencies of shift on the change of a current show that the spring from Nitinol was able to extend up to 9 (mm). The most linear character of the dependency had a coefficient of k_3=351,67 when the spring was used.

6 CONCLUSIONS

This work dealt with the design of the PNESTIFMATIC pneumatic joint, the structural solution of which was based on extending of the original patent of the hyper mobile joint. Structural solution primarily consists of the electromagnetic actuators for precise positioning. Since the main actuators work on the pneumatic principle, mechanism shows lower positioning accuracy. This work carried out simulative verification of the pneumatic bellows and experimental verification of SMA springs, which can provide an alternative to electromagnetic actuators. From the dynamic behaviour during the simulation, we have discovered that the increase of the bellow's shifts is slow and therefore it is necessary to verify the obtained results by experiment. At experimental verification of SMA springs, we have discovered that their practical usage in the PNESTIFMATIC joint's construction would be highly problematic. Despite of the fact that linearity obtained from the measured values predestines SMA springs as a suitable and easily controllable actuator, the biggest problem lies in the speed of cooling of the SMA springs (return of the material into the original state).

ACKNOWLEDGEMENT

This publication was supported by the European social fund within the framework of realizing the project „Support of inter-sectoral mobility and quality enhancement of research teams at Czech Technical University in Prague“, CZ.1.07/2.3.00/30.0034 and Slovak Scientific Grant Agency „Numerical modelling of mechatronic systems”, VEGA 1/1205/12.

REFERENCES

[1] Gregory S. Chirikjian, *Theory and applications of hyper-redundant robotic manipulators*. PhD thesis. California Institute of Technology, 1992.

[2] A. Arbor, *Snake-like Robot Conquers All Obstacles*. [online]. <http://www.redorbit.com/news/technology/139392/snakelike_robot_conquers_all_obstacles/>.

[3] J. Borenstein, G. Granosik, *Integrated Proportionally Controlled, and Naturally Compliant Universal Joint Actuator With Controllable Stiffness*. Patent No: US 6,870,343 B2. 2005.

[4] G. Granosik, J. Borenstein, Integrated Joint Actuator for Serpentine Robots. In: *IEEE/ASME Transactions on Mechatronics*, Vol. 10, No. 5., 2005. p473-481.

[5] G. Granosik, J. Borenstein, The OmniTread serpentine robot with pneumatic joint actuation. In: *Fift International Workshop on Robot Motion and Control*. 2005.

[6] D. Samek, J. Javorik, Numerical Analysis of Shape Stability of Rubber Boot. *International Journal of Mechanics*, Vol. 7, No. 3, pp. 294-301.

[7] Oliver A. Shergold, Norman A. Fleck, D. Radford, The uniaxial stress versus strain response of pig skin and silicone rubber at low and high strain rates, *International Journal of Impact Engineering* (2006), Vol. 32, pp. 1384-1402.

[8] I. Chowdhury, S. Dasgupta, Computation of Rayleigh Damping Coefficients for Large System, *The Electronic Journal of Geotechnical Engineering* (2003), Vol. 8, Bundle 8C.

[9] Detailed vibration isolation theory. Farrat isolevel Ltd. (2014) online: http://www.farrat.com

[10] Richad Q. van der Linde, *Design, Analysis, and Control of a Low Power Joint for Walking Robots, by Phasic Activation of McKibben Muscles*, IEEE Transactions on Robotics and Automation (1999), Vol. 15, No. 4, pp. 599-604.

[11] Ruiyi Tang, Dikai Liu, *An Enhanced Dynamic Model for McKibben Pneumatic Muscle Actuators*, Proceedings of Australasian Conference on Robotics and Automation (2012), Victoria University of Wellington, New Zealand.

[12] A. Gmiterko, M. Kelemen, *Miniatúrne potrubné stroje*. Košice. 2004. ISBN: 80-8073-213-2.

[13] J. Ferčec, D. Jenko, B. Buchmeister, F. Rojko, B. Budič, B. Kosec, R. Rudolf, *Microstructure of NiTi Orthodontic Wires Observations Using Transmission Electron Microscopy*, In. Metalurgija, 53(2014) 4, 469-472.

[14] Y. Toi, J.B. Lee, M. Taya, *Finite element analysis of superelastic large derformation behavior of shape memory alloy helical springs*, Computers and Structures, Publisher: Elsevier, Publishing date: June 2004, 1685-1693.